Photocatalytic soot degradation under UV and visible light

Photocatalytic soot degradation under UV and visible light

Myrthe Van Hal[1,2], Silvia Lenaerts[1,2], Sammy W. Verbruggen[1,2*]

[1] Sustainable Energy, Air & Water Technology (DuEL), Department of Bioscience Engineering, University of Antwerp, Groenenborgerlaan 171, 2020 Antwerp, Belgium

[2] NANOlab Center of Excellence, Groenenborgerlaan 171, 2020 Antwerp, Belgium

* Corresponding author. E-mail address: Sammy.Verbruggen@uantwerpen.be; telephone number: +3232653260

Abstract

Particulate matter is one of the most persistent global air pollutants that is causing health problems, climate disturbance and building deterioration. A sustainable technique that is able to degrade soot using (sun)light is photocatalysis. Currently, research on photocatalytic soot oxidation focusses on large band gap TiO_2-based photocatalysts and thus requires the use of UV light. It would prove useful if visible light, and thus a larger fraction of the (freely available) solar spectrum, could additionally be utilised to drive this process. In this work a visible light-active photocatalyst, WO_3, is benchmarked to TiO_2 under both UV and visible light. At the same time, the versatility and drastic improvement of a recently introduced digital image-based soot degradation detection method are demonstrated. An additional step correcting for non-soot related catalyst colour changes is applied, resulting in accurate detection and quantification of soot degradation for all studied photocatalysts, even for materials such as WO_3 that are inherently coloured.

With this study we aim to broaden the scope of photocatalytic soot oxidation technology to visible light-active photocatalyst. Along with this study, we provide a versatile soot degradation detection methodology based on digital image analysis that is made widely applicable.

Keywords

Photocatalysis, Soot, Visible light, Digital image analysis, Titanium dioxide, Tungsten oxide

Acknowledgments

Myrthe Van Hal acknowledges the Research Foundation–Flanders (FWO) for a doctoral fellowship (1135619N).

Authors' contributions

Myrthe Van Hal: Conceptualization, Methodology, Data acquisition, Formal analysis, Writing - original draft. **Silvia Lenaerts:** Supervision, Funding acquisition. **Sammy W. Verbruggen:** Supervision, Funding acquisition, Conceptualization, Writing - review & editing.

1. Introduction

Particulate matter (PM) is a major air pollutant, present in high concentrations in cities worldwide. It is formed by a range of both biogenic and anthropogenic processes, but the main source in populated areas is related to combustion processes (EEA 2016). High PM concentrations, including soot, have been linked to a range of health problems, both on the short and long term, such as respiratory and cardiovascular diseases. In addition, several elements of PM (*e.g.* soot, SO_4^{2-}) are known to interfere with the global climate, altering the global temperature (Thorsen et al. 2004; deRichter and Caillol 2011). Another adverse consequence of high PM (and mainly soot) concentrations is the fouling of surfaces such as buildings, statues and windows (Maury and De Belie 2010). The development of sustainable soot degrading technologies is therefore crucial. Photocatalysis is a light-driven technology that enables to degrade soot, being the carbon-based fraction of PM (Lee and Choi 2002; Lee et al. 2004; Mills et al. 2006; Chin et al. 2007, 2009; Smits et al. 2013; Van Hal et al. 2019; Pozo-Antonio et al. 2020). When light with sufficient energy reaches the surface of a semiconductor, electron-hole pairs are formed. These electron-hole pairs can participate in oxidation-reduction reactions, and in the presence of carbonaceous soot particles ultimately result in their mineralisation towards CO_2 (Chin et al. 2009).

Current research mainly focusses on the large band gap material TiO_2, that exclusively requires UV light (Lee and Choi 2002; Lee et al. 2004; Mills et al. 2006; Chin et al. 2007; Smits et al. 2014; Kameya et al. 2017; Pozo-Antonio et al. 2020), while visible light-active photocatalysts, characterized by a smaller band gap, remain largely unstudied in the context of soot degradation. In order to apply photocatalysis as a sustainable energy-efficient soot abatement technology, the ability of this process to utilise visible light (and eventually sunlight) is crucial. In addition, as research on the use of visible light-active photocatalysts (often WO_3) in other research areas (*e.g.* water and air purification)(Kim and Choi 2011; Chen et al. 2012; Zhang et al. 2012; Fukumura et al. 2017; Xie and Ouyang 2017; Peeters et al. 2020; Van Hal et al. 2021) increases, the capacity of these materials to cope with deposited soot is an important parameter for the application of these materials in urban (highly soot-contaminated) areas.

In this study, the soot degrading properties of both commonly studied TiO_2 and partially visible light-active WO_3 are investigated, both using UV and visible light. To the best of our knowledge this is the first time WO_3-based photocatalysts are studied for photocatalytic soot oxidation. The analysis of visible light-active photocatalysts for soot degradation is complex, in the sense that typically sensitive and expensive equipment would be required to, for instance, measure weight losses upon degradation (Chin et al. 2009). Visible light-active photocatalysts are typically coloured materials (*e.g.* WO_3 is green-yellow), which complicates alternative optical detection strategies. In this work we have therefore improved a low-cost and time-efficient digital image analysis method, as presented in our earlier work (Van Hal et al. 2019), by correcting for changes in the intrinsic colour of the catalysts during the degradation experiment. In this way we applied this versatile detection tool for the first time to study coloured samples. Additional information on the ongoing reactions is collected using an *in-situ* FTIR reaction cell. Combination of the image analysis method and *in-situ* FTIR cell allowed us to easily compare the studied photocatalysts, both considering their short- and long-term soot oxidation capacity, as well as the by-products that were produced (and thus determine the overall mineralisation efficiency). Eventually, the aim of this study is three-fold: i) expand the knowledge on photocatalytic soot oxidation using visible light-active photocatalysts, ii) expand the knowledge on photocatalytic soot oxidation using visible light and iii) in doing so improve and expand the applicability of a versatile image analysis methodology to coloured samples.

2. Experimental

2.1 Photocatalyst synthesis, coating and characterisation

WO_3 nanopowder, further denoted as $WO_{3\ Mart.}$, was synthesized according to a precipitation method described by Martínez-de la Cruz *et al.* (Martínez and Cuéllar 2010). In short, Ammonium tungstate hydrate (99.99%, Aldrich, prod. Japan) was dissolved in deionised water at 80°C, after which nitric acid (65%, Chem Lab, Belgium) was added. The tungstate solution was kept at 80°C for 70 minutes and the formed precursors were decomposed by heating the obtained precipitates 3 hours at 600°C.

Commercially available P25 was obtained from Evonik (Germany), PC500 from Cristal Activ (France) and WO_3 nanopowder (<100 nm) was obtained from Sigma Aldrich (prod. China), further denoted as $WO_{3\ Sigma}$). All powders were used as such in further experiments.

The photocatalysts were drop casted on cleaned soda lime glass slides (2.5 cm by 1.5 cm, VWR, prod. China). To this end, suspensions were made of the catalyst powders in methanol (99,8%, Chem Lab, Belgium) at a concentration of 67 mg mL^{-1}. The suspensions were ultrasonicated for 1 h and applied onto the slides so a coverage of 3.5 mg cm^{-2} was obtained. The coated glass slides were dried for 2h in air, and then at 80°C overnight to remove residual solvent. Soot (Printex-U, Evonik, Germany) was drop casted on top of the photocatalyst layer, from a suspension containing 1 mg mL^{-1} in methanol, so a soot coverage of 0.022 mg cm^{-2} was obtained. and the glass slides were again dried to remove all residual solvent. This method thus ensures a direct physical contact between the soot particles and the photocatalyst layer.

A range of physico-chemical characterisation techniques was performed to confirm correct synthesis of the WO_3 nanopowder ($WO_{3\ Mart.}$). UV-VIS spectroscopy was performed using a Shimadzu UV-2600 spectrophotometer with integrated sphere. The band gap was determined using a Tauc plot. A Micromeritics Tristar 3000 surface area & pore size analyser was used to determine the specific surface area and porosity. A Bruker D8 Advanced diffractometer was used to determine the crystalline structure (Cu $K\alpha$ radiation; 40 kV; 40 mA; 20-80 degrees; 0.5 s $step^{-1}$). In addition, energy dispersive X-ray fluorescence (EDXRF) measurements were performed using a Minipal spectrometer of PANalytical (30 kV; 3-5 µA).

2.2 Colour-based monitoring of photocatalytic soot oxidation

Soot degradation was monitored using the image analysis method described by Van Hal *et al*. (2019), to which the reader is kindly referred for a more elaborate description of the methodology. In short, this method quantifies the extent of soot degradation by the discolouration of a surface using digital

images. For the experiment under UV light, the previously prepared samples were placed 3 cm under a Philips fluorescence S 25 W UVA lamp obtaining an incident light intensity of 2.1 mW cm^{-2} over the wavelength region 290 - 400 nm (λ_{max} at 354 nm), as measured by a calibrated spectroradiometer (Avantes Avaspec-3648-USB2). For the experiment under visible (VIS) light the samples were placed 2.5 cm under a blue LED-array (Roithner LaserTechnik) obtaining an incident light intensity of 14 mW cm^{-2} in the wavelength region 390 - 470 nm (λ_{max} at 422 nm). The irradiance spectra can be obtained from the Supporting Information section (Fig. S1).

A standardised custom-made 'photobox' was used to ensure a constant and homogeneous background illumination, of which the detailed specifications can be retrieved elsewhere (Smits et al. 2013). Pictures were taken using a Canon Eos 500D camera, positioned 20 cm above the samples, in manual mode (iso 200, aperture f8 and focal exposure 1:5) at maximal resolution (5184×3456) at 72 dpi. The free image software ImageJ was used to process the pictures. The L* coordinate of the CIELab colour space, which quantifies the brightness of the sample, was used as a measure of the amount of soot deposition and was set to vary between 0 (black) and 100 (white). The shift of the most frequent L* value was used to quantify the amount of soot degradation of the shallow soot haze that is smeared over the surface of the samples. The degradation of concentrated soot spots was quantified by the decrease of the height of the darkest peak (*i.e.* at low/dark L* values). A more detailed description of this data processing method is given in earlier work (Van Hal et al. 2019).

Each photocatalyst was applied on five glass slides. Soot was deposited on four of them (samples consisting of photocatalyst layer + soot are further denoted as 'standard' samples), of which three glass slides were illuminated and one was kept in the dark as negative control. The glass slides containing only photocatalyst were illuminated together with the standard samples, in order to correct for colour changes at the level of the catalyst itself. Photographs were taken from the glass slides before and after soot deposition at specific UV illumination intervals (0, 5, 11, 20, 26, 40, 61 and 82 days). Corrections for possible deviations caused by small changes in the background illumination

were made by processing a set area of the background in ImageJ and applying the hereby obtained deviation in L* value to the complete dataset of that time point.

A second, additional optical detection method (absorbance method) was performed at the same time points. The decrease in absorbance of the sample surface, as a result of soot degradation, was quantified using a spectroradiometer (Avantes Avaspec-3648-USB2) and converted to a soot haze degradation percentage as described in our previous study (Van Hal et al. 2019).

2.3 *In situ* monitoring of photocatalytic soot oxidation

Insight into the photocatalytic reactions occurring at the sample surface was gathered using an *in-situ* FTIR method. In summary, 5 mg of a 0.6 wt% solid powder soot (Printex-U)-photocatalyst mixture were added to 115 mg KBr (99.7%, VWR, Belgium) and pressed for 2 minutes at 5 tonnes, obtaining a round flat IR-transparent pellet. This pellet was positioned in the centre of the reaction cell, of which the specifications are detailed elsewhere (Van Hal et al. 2019). The cell was flushed with air (200 mL min^{-1}) until a stable readout was obtained and sealed airtight. The pellet was illuminated by eight LEDs at each side placed in a circular pattern (10 mW each, Roithner LaserTechnik). The UV-LEDs resulted in an incident intensity of 330 µW cm^{-2} in the wavelength region 350 - 420 nm (λ_{max} at 377 nm), whereas the blue VIS-LEDs reached an incident intensity of 400 µW cm^{-2} in the wavelength region 390 - 470 nm (λ_{max} at 425 nm).

3. Results and discussion

3.1 Characterisation

The photocatalysts selected for this study (P25, PC500, $WO_{3\ Sigma}$ and $WO_{3\ Mart.}$) have already been extensively described in literature, or by the respective manufacturers (Sanchez-Martinez et al. 2013). Nonetheless, to confirm correct synthesis of the photocatalyst prepared in the lab, a series of physico-chemical characterisation experiments (N_2 sorption, UV-VIS spectroscopy, X-ray diffraction and energy dispersive X-ray fluorescence) was performed. An important difference between TiO_2- and WO_3-based

photocatalysts is their band gap. P25 (3.2 eV) and PC500 (3.3 eV) are large band gap materials, while both WO_3-based photocatalysts have a smaller band gap (2.6 eV), resulting in partial visible light activity. Both WO_3-based photocatalysts have a small surface area (< 10 m^2 g^{-1}), while P25 has an intermediate surface area (52 m^2 g^{-1}), and PC500 is a large surface area material (295 m^2 g^{-1}). The measured photocatalyst properties correspond very well with earlier reports, thus confirming the reproducibility of these samples (Van Hal et al. 2021).

3.2 Colour-based monitoring of photocatalytic soot oxidation

Both selected optical detection methods (digital image analysis, and the absorbance method) were applied to 'white' TiO_2- and (yellow-greenish-)coloured WO_3- based photocatalysts. A negative control (*i.e.* standard sample kept in dark) was added to confirm all changes were induced by illumination (Fig. S2). A glass slide coated only with photocatalyst (no soot, 'light-control' sample) was kept under each light source together with the standard samples, to allow for a correction of changes in the intrinsic colours of the photocatalysts themselves throughout the experiments.

Using the digital image analysis method, a graph is obtained showing the number of pixels of each L*-coordinate. When applying this to the light-control samples for P25, $WO_{3\ Sigma}$ and $WO_{3\ Mart.}$, Fig. 1 is obtained, thus reflecting the changes in colour of the photocatalysts themselves, in the absence of soot deposits.

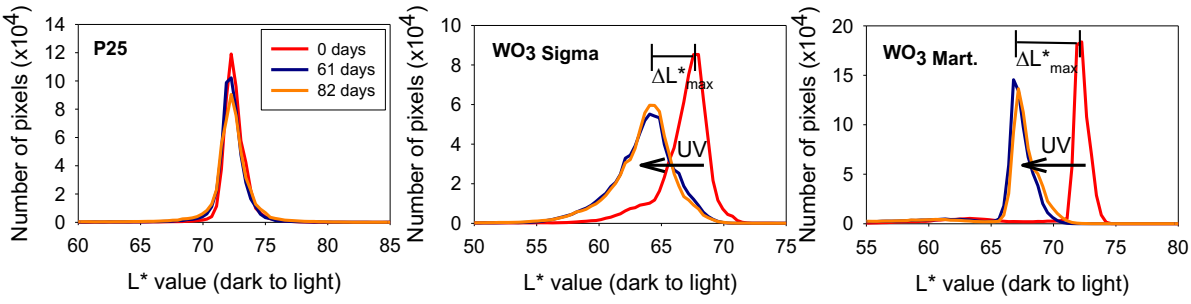

Fig. 1 UV light experiment: Number of pixels plotted against the L* value for a glass slide solely coated with (left) P25, (middle) $WO_{3\ Sigma}$ and (right) $WO_{3\ Mart.}$, representing the UV-induced colour change of the photocatalyst surface itself upon UV illumination

A clear colour shift to lower L* values can be observed for both WO_3-based photocatalysts, thus reflecting darkening of the bare photocatalyst surface induced by the UV illumination. This colour change arises from decreasing amounts of water adsorbed on the (coloured) photocatalyst surface, resulting from a combination of photocatalytic (adsorbed) water oxidation and water evaporation upon illumination of the surface. This was supported by the observation of similar darkening of the photocatalyst surface after drying of the light-control samples, as illustrated in the Supporting information section (Fig. S3). As both the digital image analysis and absorbance method are optical detection methods, this photocatalyst colour change will also contribute to the results of the standard samples with soot and might give rise to false interpretations of the degradation efficiency. It is therefore vital to correct for this effect. In contrast, this UV-induced photocatalyst discolouration was not seen for the white photocatalysts (*i.e.* P25, PC500, Fig. 1).

For the absorbance method, the change in absorbance value attributed to illumination-induced colour changes of the pure photocatalyst can be converted to a theoretical equivalent soot degradation efficiency according to (Eq. 1), that can be used to correct the results of the standard samples.

$$\textit{Eq. PC soot degradation efficiency pure photocatalysts (\%)} = \left(\frac{-A_{NS,t}}{A_0}\right).100 \qquad \text{(Eq.1)}$$

Where $A_{NS,t}$ represents the absorbance value of the light-control sample (no soot) at a specific time point and A_0 is the absorbance value of a standard sample (photocatalyst with soot on top) at the beginning of the experiment (no illumination = completely fouled glass slide). All absorbance values were taken at 600 nm.

When applying (Eq. 1) to the light-control samples of P25, $WO_{3\ Sigma}$ and $WO_{3\ Mart.}$ of the UV-experiment, Fig. 2 is obtained.

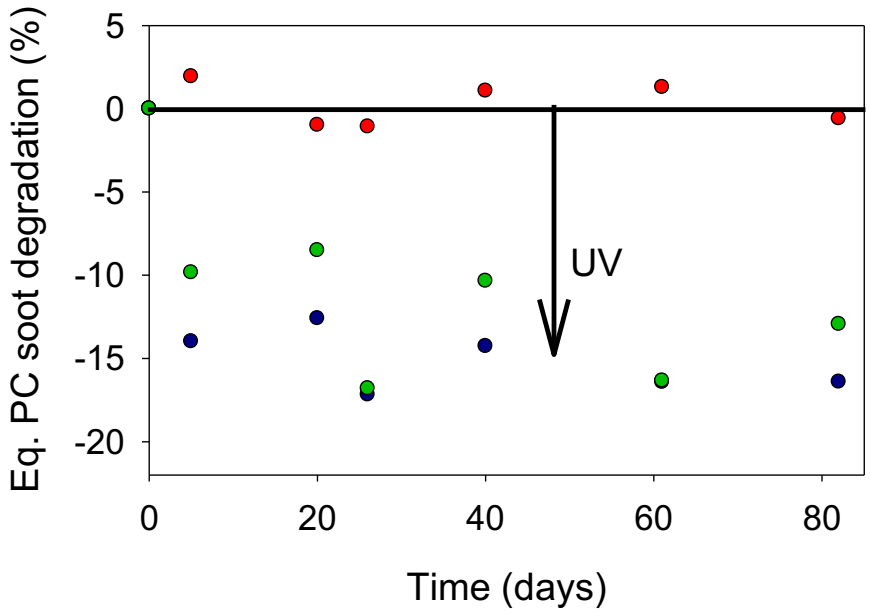

197

198 **Fig. 2** UV light experiment: UV-induced darkening of photocatalyst surface expressed as theoretical equivalent soot
199 degradation efficiency for P25 (red), $WO_{3\ Sigma}$ (blue) and $WO_{3\ Mart.}$ (green) determined using the absorbance method, as a
200 function of UV illumination time

201 From Fig. 2 it can be seen that for P25 the theoretical equivalent soot degradation efficiencies fluctuate
202 around 0% soot degradation, again evidencing the absence of colour changes for the 'white'
203 photocatalysts. The slight variation in these data can be ascribed to small variations in the position of
204 the sampling probe, as the same noisiness is encountered for all measured samples (both in dark and
205 under UV illumination). When interpreting the data of both WO_3-based photocatalysts, a clear negative
206 theoretical equivalent soot degradation percentage (ranging between -10% and -17%) is present for
207 all time points after initiation of the UV illumination. This negative equivalent soot degradation again
208 reflects the UV-induced darkening of the photocatalyst surface, thus confirming the results from the
209 digital image analysis method.

210 A similar illumination-induced photocatalyst discolouration was also observed under visible light. To
211 correct for this illumination-induced photocatalyst colour change in the image analysis method, an
212 additional processing step should be added. In this case, the 'number of pixels *vs.* L* value' plots of the
213 standard samples need to be shifted an equal distance corresponding to ΔL^*_{max}, (see Fig. 1) in the
214 opposite direction of the discolouration before determining the position of the L^*_{max} value, that

corresponds to the final amount of soot. In the absorbance method the soot degradation efficiencies were corrected for the illumination-induced shift by subtracting the negative theoretical equivalent soot degradation efficiencies. The results obtained in the UV-experiment with the original and corrected image analysis and absorbance method are presented in Fig. 3.

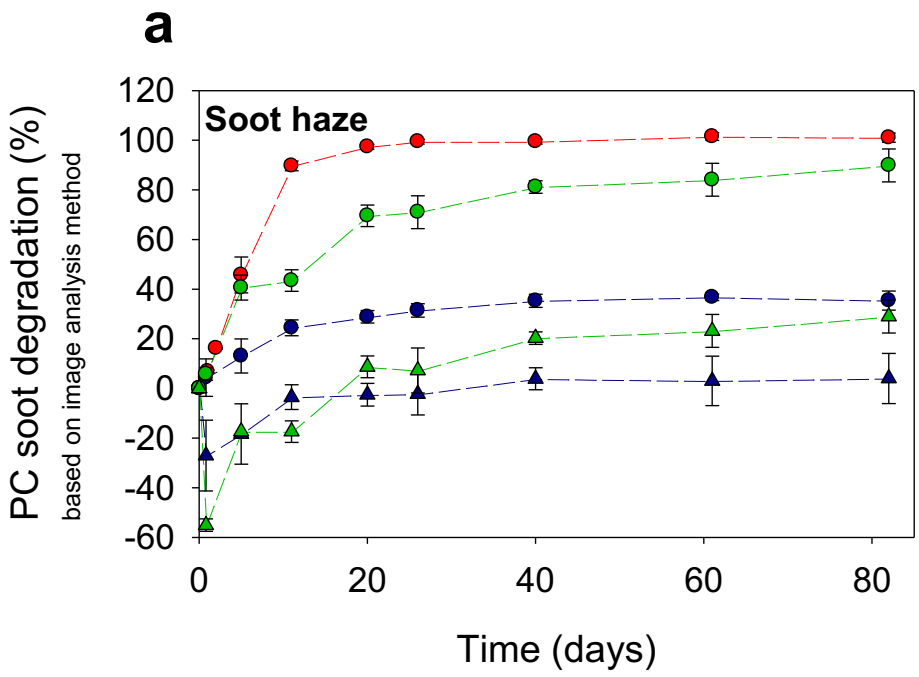

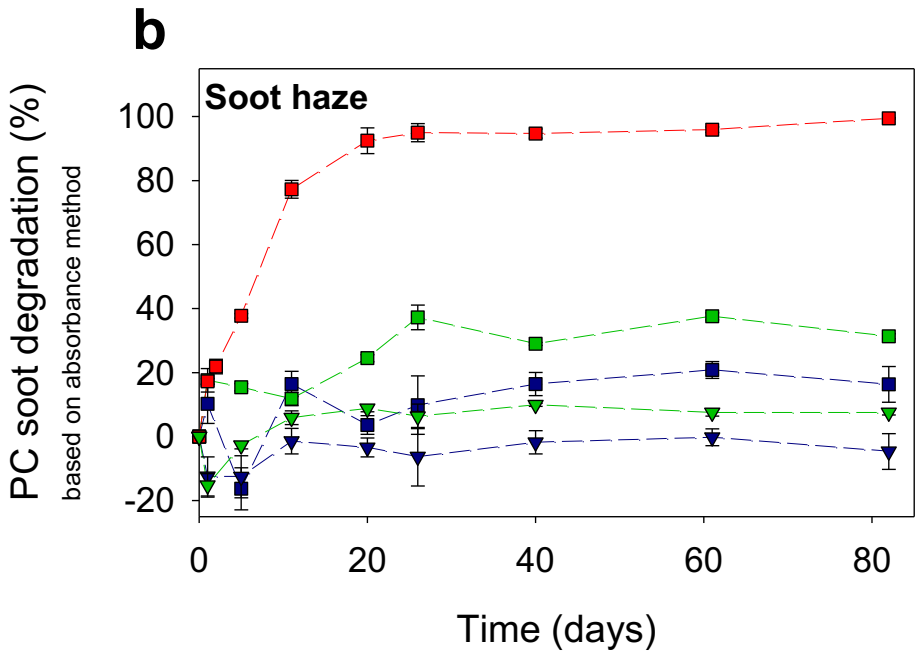

Fig. 3 UV light experiment: Photocatalytic degradation of uniform soot haze by P25 (red), $WO_{3\ Sigma}$ (blue) and $WO_{3\ Mart.}$ (green), as a function of UV illumination time: a) Comparison of original (▲) and corrected (●) digital image analysis method and b)

comparison of original (▼) and corrected (■) absorbance method. For P25 the original values equal the corrected, as no correction was required (no discolouration of photocatalyst). The error bars are based on standard deviation for three independent samples. Dashed lines are added to guide the reader's eye

In Fig. 3 the UV-induced darkening of the photocatalyst surface is reflected in the (initial) negative photocatalytic soot degradation percentages obtained by both original methods for both WO_3-based photocatalysts. An additional data processing step was implemented for both methods correcting for this illumination-induced photocatalyst colour change, as described in the previous paragraph. It can be seen that for both WO_3-based photocatalysts (as opposed to the results for P25) large deviations arise between both different (corrected) detection methods. After 82 days almost complete degradation (90%) of the soot haze by $WO_{3\ Mart.}$ was measured using the corrected image analysis method, whereas the corrected absorbance method only appeared to detect 31% degradation. Overall, much lower degradation efficiencies were measured using the corrected absorbance method for both WO_3-based photocatalysts compared to the results obtained with the corrected image analysis method. When looking at the actual degradation of the soot haze with $WO_{3\ Mart.}$ (Figure 4) almost complete degradation is observed after 82 days as the colour of the surface again equals the colour of the pristine photocatalyst at that UV illumination time (as in the case of 'No soot'), which is not the case at the other time points. Thus, while the absorbance method is able to accurately determine the degradation of the soot haze for non-coloured (*i.e.* white) photocatalysts (*e.g.* P25, PC500), this is clearly not the case for the studied coloured photocatalysts (WO_3). As the image analysis allows visualization of the complete soot degradation process (over all L* values), the illumination-induced change in colour (in this case darkening) of the photocatalyst can be studied independently from the illumination-induced (photocatalytic) soot degradation (and thus brightening). In the absorbance method, however, all occurring visual changes are contained in a single output value (*i.e.* the absorbance of the entire surface), and as a result both phenomena cannot be disentangled. Therefore, digital image analysis is much more reliable for studying soot degradation over coloured photocatalysts (or by extension coloured surfaces) compared to the absorbance method. For this reason, only the digital image analysis method will be used further in this study.

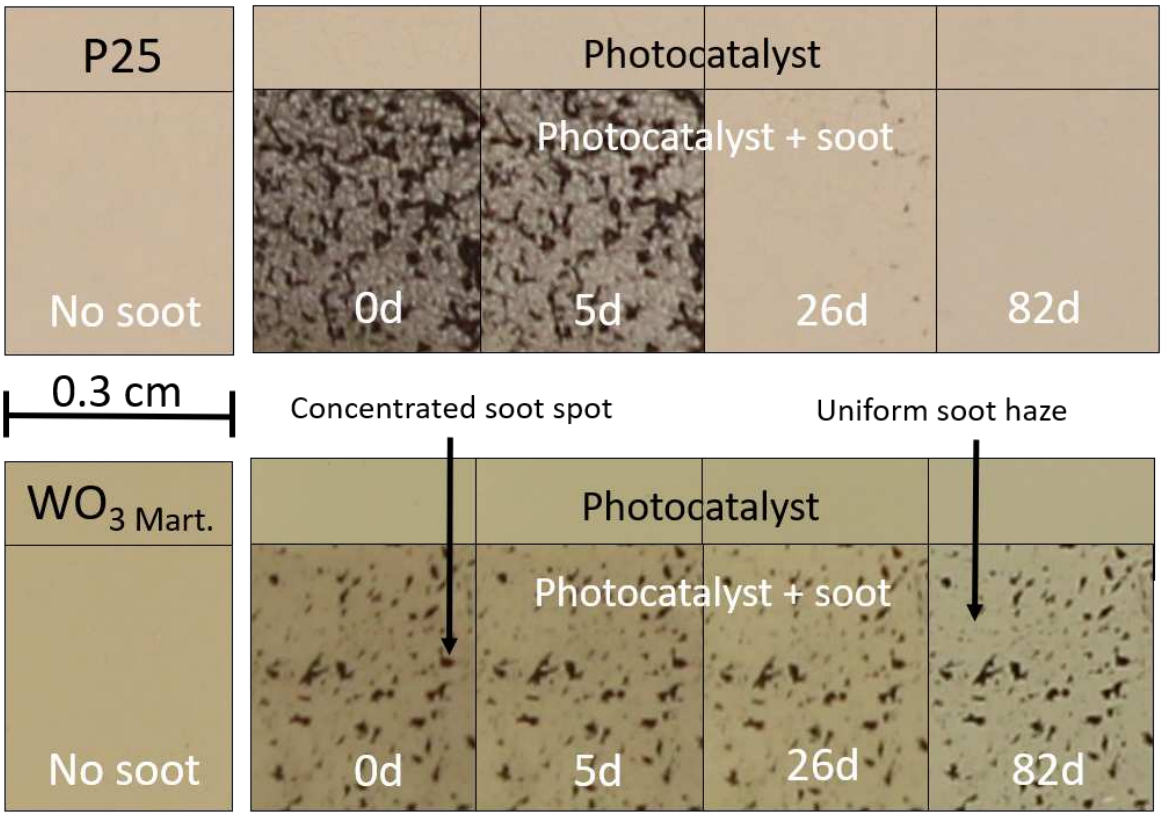

Fig. 4 UV light experiment: Subsequent digital images of the photocatalytic soot degradation on a glass slide coated with (top) P25 and (bottom) $WO_{3\ Mart.}$ with f.l.t.r. a glass slide without soot, with soot before UV illumination, and after 5, 26 and 82 days of illumination

The results of the UV-experiment obtained with the corrected digital image analysis method are shown for all photocatalysts and the glass slide containing solely soot in Fig. 5.

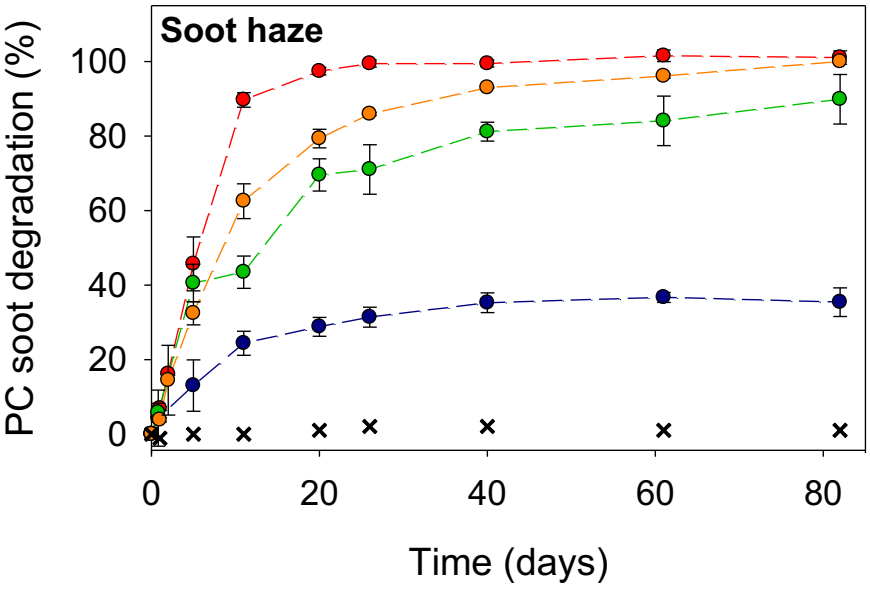

Fig. 5 UV light experiment: Photocatalytic soot degradation of the soot haze by P25 (red), PC500 (orange), $WO_{3\ Sigma}$ (blue) and $WO_{3\ Mart.}$ (green) determined using the improved digital image analysis method after light-induced colour-change correction, as a function of UV illumination time. The result of the glass slide solely coated with soot is shown by black crosses (X). The error bars are based on three independent samples. Dashed lines are added to guide the reader's eye

It is clear that P25 is the fastest photocatalytic soot degrader of all studied materials, achieving complete soot degradation after 40 days of UV illumination. It should be noted that the applied soot quantity (22 µg cm^{-2}) is high compared to outdoor (urban) soot concentrations (mean elemental carbon deposition of 1.1 µg cm^{-2} $year^{-1}$) (Chabas et al. 2008), thus requiring a much shorter illumination time to obtain complete degradation of real outdoor soot depositions. As soot deposition is a gradual process, soot loadings on existing surfaces reach values as used in this study after many years to decades of exposure (Ferrero et al. 2020). Photocatalytic soot degradation by the other photocatalysts occurred at a more gradual pace. It took PC500 82 days to completely degrade the soot haze. Around 90% oxidation of the uniform soot haze was obtained by $WO_{3\ Mart.}$ after 82 days, while the commercially available WO_3 nanopowder ($WO_{3\ Sigma}$) was only able to degrade around 35% of the soot haze by the end of the experiment. All studied photocatalysts display a fast initial soot degradation rate, slowing down at higher soot degradation percentages, thus resembling first order kinetics as previously described in literature for P25 (Mills et al. 2006; Chin et al. 2007; Smits et al. 2013, 2014; Van Hal et al. 2019).

An interesting additional feature of the image analysis method is that it also enables to separately determine the degradation efficiency of pertinent concentrated soot spots. The results of the degradation of the concentrated soot spots in the UV-experiment are shown in Fig. 6.

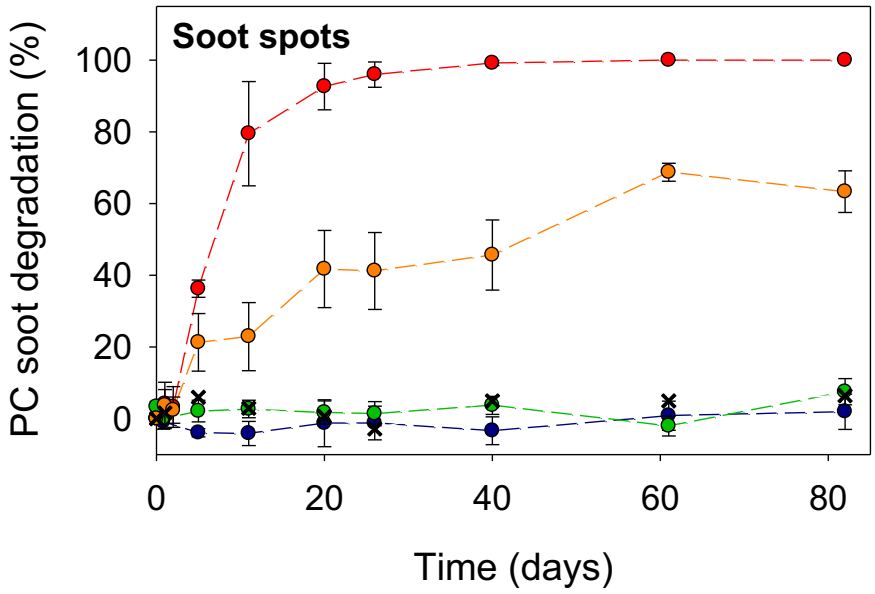

278

279 **Fig. 6** UV light experiment: Photocatalytic degradation of concentrated soot spots by P25 (red), PC500 (orange), $WO_{3\ Sigma}$
280 (blue) and $WO_{3\ Mart.}$ (green) determined by digital image analysis, as a function of UV illumination time. The result of the glass
281 slide solely coated with soot is shown by black crosses (X). The error bars are based on three independent samples. Dashed
282 lines are added to guide the reader's eye

283 When examining the photocatalytic degradation of the concentrated soot spots (Fig. 6), it can be seen
284 that P25 was able to fully degrade the concentrated soot spots after 61 days, somewhat slower than
285 the uniform soot haze. After 82 days, at the end of the experiment, *ca*. 65% of the soot spots were
286 degraded by PC500. Only very little degradation of the concentrated spots was measured for purely
287 WO_3-based photocatalysts. At the end of the experiment (82 days) only 1.5% of the soot spots were
288 degraded by $WO_{3\ Sigma}$, while $WO_{3\ Mart.}$ reached 7% degradation. A striking difference is thus apparent
289 for both WO_3-based photocatalysts when comparing the good degradation capacity for a soot haze
290 *versus* the poor efficiency towards concentrated soot spots.

291 With direct oxidation being acknowledged as the main photocatalytic soot oxidation mechanism (Lee
292 and Choi 2002), the characteristics of the photocatalyst-soot surface area are crucial in determining
293 the soot degradation rate. As mentioned, both WO_3-based photocatalysts have a very small BET
294 surface area (< 10 $m^2\ g^{-1}$), PC500 on the other hand is known for its large surface area (~ 300 $m^2\ g^{-1}$),
295 and the surface area of P25 lies in-between (~ 50 $m^2\ g^{-1}$). The low photocatalytic soot oxidation rate

296 of both WO_3-based photocatalysts might thus be related to their low surface area. When considering
297 both TiO_2-based photocatalysts, the best result was obtained with P25, even though it does not possess
298 the largest surface area. Both TiO_2-based photocatalysts are characterised by a vastly different crystal
299 structure. While P25 is known to consist of an optimised anatase:rutile ratio, PC500 consists of pure
300 anatase and a small amorphous fraction. In addition, PC500 has a smaller primary particle size, and
301 smaller particles are known for faster electron-hole recombination (Deng et al. 2002). The known poor
302 electronic properties of PC500 (Keulemans et al. 2016) might thus contribute to the lower soot
303 degradation capacity of this material compared to P25. As penetration of soot into the photocatalyst
304 layer is negligible, it has been shown that the photocatalytic soot oxidation rate only depends on the
305 thickness of the photocatalyst layer up to a thickness in the range of the diffusion length of the excited
306 carriers (Luttrell et al. 2014). In this study, thick photocatalyst layers were applied (3.5 mg cm^{-2}), as also
307 evidenced by Fig. 4, thus excluding layer thickness as an influencing factor. In addition, drop casting of
308 both photocatalyst and soot on glass slides results in rough films, excluding surface roughness as
309 decisive factor for the performed experiments.

310 Another important difference between the WO_3-based and TiO_2-based photocatalysts is their band
311 gap. The smaller band gap of WO_3 allows at least partial utilisation of visible light and thus a larger
312 fraction of the solar spectrum, making it a promising material for use in energy-efficient environmental
313 remediation processes. To study this effect, the experiments were repeated with a visible light blue
314 LED source using the best performing TiO_2-based photocatalyst (P25) and both WO_3-based
315 photocatalysts ($WO_{3\ Sigma}$ and $WO_{3\ Mart.}$). The results of the VIS light-experiment are shown in Fig. 7. The
316 result of the glass slide solely covered with soot (without photocatalyst) is shown in the Supporting
317 information section (Fig. S4).

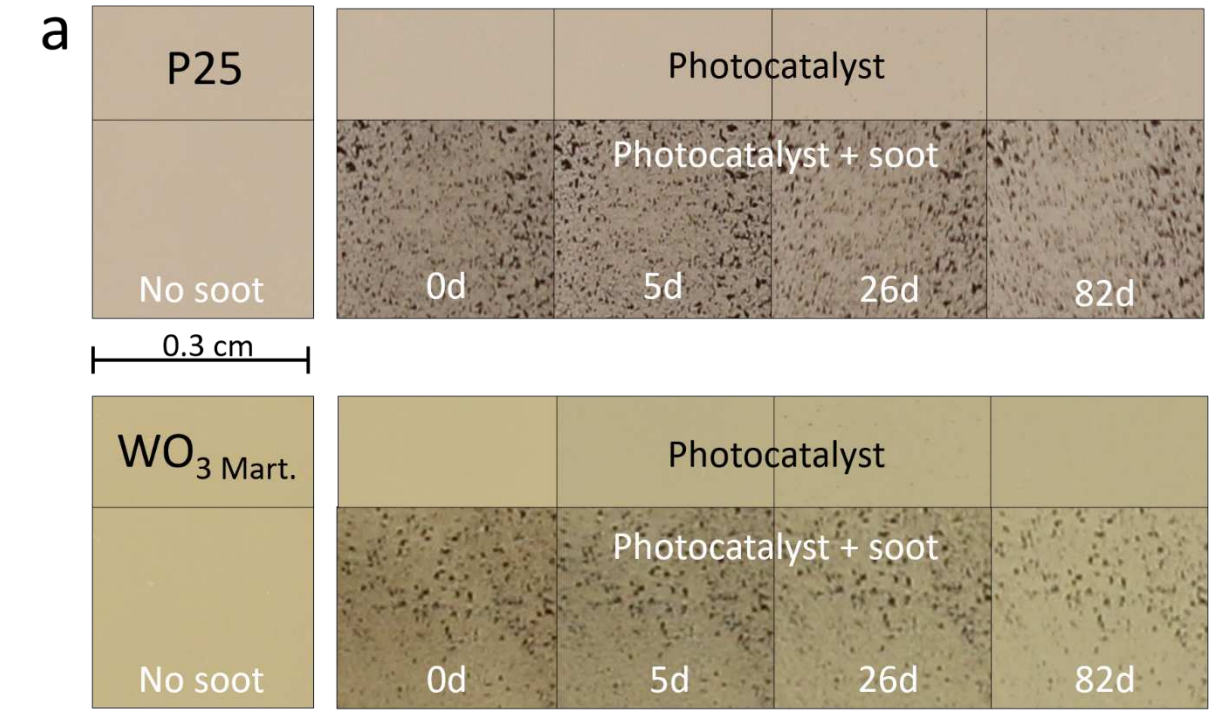

318

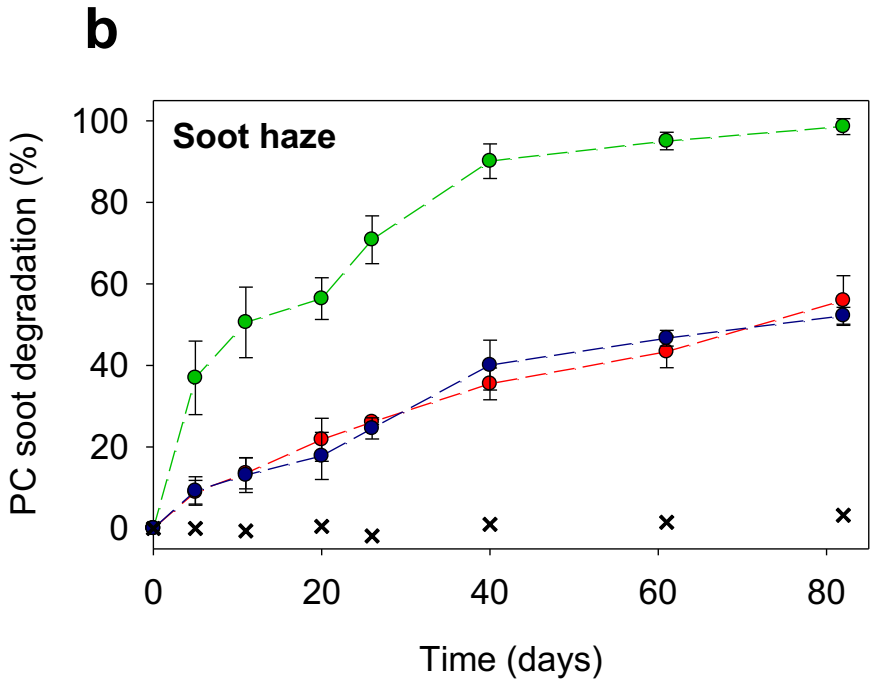

319

320 **Fig. 7** VIS light experiment: a) Subsequent digital images of the photocatalytic soot degradation on a glass slide coated with
321 (top) P25 and (bottom) $WO_{3\ Mart.}$ with f.l.t.r. a glass slide without soot, with soot before VIS light illumination, and after 5, 26
322 and 82 days of illumination. b) Photocatalytic soot degradation of a uniform soot haze by P25 (red), $WO_{3\ Sigma}$ (blue) and WO_{3}
323 $_{Mart.}$ (green) determined using the improved digital image analysis method after light-induced colour-change correction, as a
324 function of visible light illumination time. The result of the glass slide solely coated with soot is shown by black crosses (X).
325 The error bars are based on three independent samples. Dashed lines are added to guide the reader's eye

From Fig. 7 it is clear that under VIS light illumination $WO_{3\ Mart.}$ is the fastest soot degrader, reaching complete oxidation of the uniform soot haze after 82 days. Both other photocatalysts degrade the soot haze slower under these conditions, as P25 is only able to degrade 56% of the haze after 82 days, and $WO_{3\ Sigma}$ reached 52% degradation by the end of the experiment.

Despite the large band gap of P25 (3.2 eV) still significant soot haze degradation is observed under the VIS light lamp, which has also been previously observed in literature (Verbruggen et al. 2016; Rosli et al. 2018). This can mainly be attributed to the small, yet existing, overlap of the absorbance band of P25 and the irradiance spectrum of the VIS light source (see Fig. S1). This allows P25 to effectively use a small part of the light emitted by the VIS light lamp over the entire duration of the long-term experiment. For the WO_3-based photocatalysts (band gap = 2.6 eV) a more optimal overlap exists between the photocatalyst absorbance band and the light emission spectrum (Fig. S1), allowing WO_3-based photocatalysts to potentially use a larger fraction of the light emitted by the VIS light lamp. The advantage of WO_3 when using visible light is clear from Fig. 7, with $WO_{3\ Mart.}$ clearly outperforming P25 and reaching complete oxidation after 82 days (*vs.* 90% under UV light), even despite its low surface area.

The short- and long-term performance of the studied photocatalysts using the two different light sources, expressed in photonic efficiency (PE), is summarised in Table 1. The PE is defined as the ratio of the photocatalytic reaction rate (degraded carbon molecules s^{-1}) over the incident photon flux (photons s^{-1}) (Braslavsky et al. 2011; Smits et al. 2013). The carbon degradation rate was derived from the percentage of soot haze degradation after a certain period of illumination, taking into account the carbon content of Printex-U (95.56%) (Smits et al. 2013) and the initial quantity of soot on the sample (22 µg cm^{-2}). In this way, the lower limit of the PE was calculated, as part of the soot is also present in concentrated soot spots that cannot be accounted for in this calculation. The light intensities were measured with a spectroradiometer, obtaining an incident photon flux of 4.22 x 10^{15} photons s^{-1} cm^{-2} for the UV lamp and of 3.10 x 10^{16} photons s^{-1} cm^{-2} for the VIS light lamp (between 290 and 800 nm)

over an illuminated surface of 3.8 cm^2. The results again evidence that under UV light P25 outperforms both WO_3-based photocatalysts, both on short and long term, while under VIS light the best results are obtained using $WO_{3\ Mart.}$. The photonic efficiencies obtained with P25 under UV light are 12-67 times higher than those under VIS light, while for the WO_3-based photocatalysts the PEs only dropped by a factor 5-11 when using VIS instead of UV light, reflecting the higher capability of WO_3 to utilise VIS light.

Table 1. Lower limit of photonic efficiency based on the degradation of the soot haze, of the studied photocatalysts after different illumination times for both a UV and a VIS light lamp

	PE after 5 days ($x10^{-5}$)		PE after 82 days ($x10^{-5}$)	
	UV light	**VIS light**	**UV light**	**VIS light**
P25	47.5	0.7	3.4	0.3
$WO_{3\ Sigma}$	7.5	0.7	1.2	0.2
$WO_{3\ Mart.}$	23.7	2.9	3.2	0.5

The degradation of the concentrated soot spots under VIS light illumination is shown in Fig. 8.

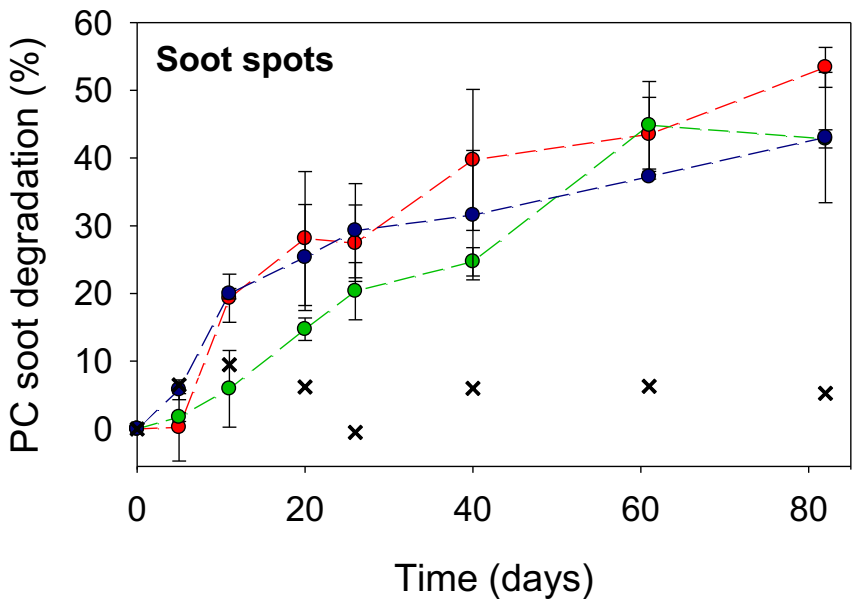

Fig. 8 VIS light experiment: Photocatalytic degradation of concentrated soot spots by P25 (red), $WO_{3\ Sigma}$ (blue) and $WO_{3\ Mart.}$ (green) determined by digital image analysis, as a function of visible light illumination time. The result of the glass slide solely coated with soot is shown by black crosses (X). The error bars are based on three independent samples. Dashed lines are added to guide the reader's eye

From Fig. 8 it is clear that all three photocatalysts result in similar degradation of the concentrated soot spots under VIS light. P25 slightly outperformed both WO_3-based photocatalysts, obtaining 53% degradation after 82 days for P25 and 43% degradation for both WO_3-based photocatalysts. This is in contrast to what was seen in the UV light experiment, where almost no (< 7%) degradation of the soot spots was attained by both WO_3-based photocatalysts. Again, the smaller band gap of WO_3 results in improved performance of these photocatalysts when using VIS light instead of UV light.

3.3 *In situ* monitoring of photocatalytic soot oxidation

The image analysis method allows to simultaneously monitor degradation of both soot haze and concentrated soot spots, but provides no information on the ongoing processes, nor the formation of possible intermediates and end products. To complement the results of the image analysis method, an *in situ* FTIR reaction cell was used in this second part of the study.

Blank tests (no soot) were performed as negative control, showing no CO_2 evolution in the absence of soot under UV illumination (Supporting information Fig. S5). Experiments with soot-photocatalyst-KBr pellets under UV light clearly revealed CO_2 evolution for all studied photocatalysts, evidenced by the signal in the wavenumber range 2290-2390 cm^{-1} (ν_{as}(O=C=O)). The IR spectra after 10 hours of UV illumination are presented in Fig. 9a for PC500 and $WO_{3\ Mart.}$ and in Supporting information for the other photocatalysts (Fig. S6). Oxygen depletion in the airtight reaction cell results in saturation of soot oxidation after *ca*. 10 h (Van Hal et al. 2019), resulting in flattening of the CO_2 evolution curve after this time point. A second significant band can be observed in the wavenumber range 1273-1445 cm^{-1} with two maxima at 1360 (ν_s(COO)) and 1380 cm^{-1} (δ(CH)). This band can be ascribed to formate adsorbed on the photocatalyst surface, $CHOO^-_{(ad)}$ (Hauchecorne et al. 2011), and was observed for all studied materials. Steric hindrance possibly masks other bands attributed to this compound as it is adsorbed to the surface. These results suggest that the hypothesis of Chin and co-workers from 2009 (Chin et al. 2009), originally presented for TiO_2, is also valid for WO_3-based photocatalysts. This

hypothesis states that soot can be photocatalytically oxidised via two soot oxidation pathways, either through direct oxidation to CO_2, or via a sequential mechanism involving a variety of intermediates (Chin et al. 2009). The IR spectrum of PC500 contained an additional band that was not detected for the other photocatalysts, located between 1483 and 1783 cm^{-1} with a maximum near 1665 cm^{-1} (ν(C=O)). This band can be ascribed to adsorbed formate-related products such as formaldehyde ($CH_3OOH_{(ad)}$) and methyl formate ($HCHO_{(ad)}$)), evidencing the largely incomplete oxidation of soot when using PC500. The degradation of soot can be monitored by the generation of two negative bands centred around 2848 and 2922 cm^{-1}, reflecting the disappearance of C-H stretching vibrations. The production of both CO_2 and adsorbed formate as a function of UV illumination time are shown in Fig. 9b.

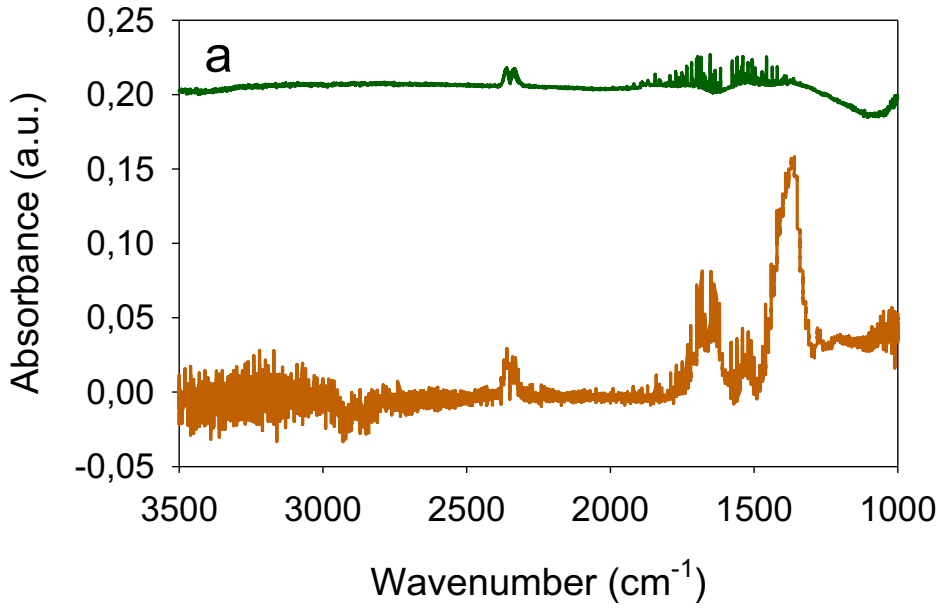

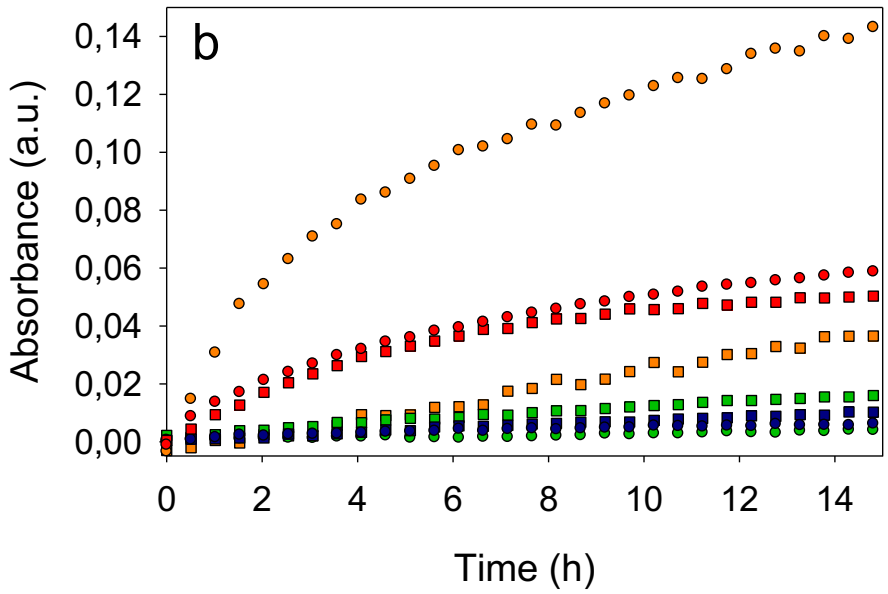

Fig. 9 UV-experiment: a) FTIR spectra of soot-photocatalyst-KBr pellet in *in situ* reaction cell after 10 hours of UV illumination for PC500 (orange) and $WO_{3\ Mart.}$ (green). Positive bands represent product formation, negative bands point at the degradation of soot. b) Evolution of CO_2 (■) and formate (●) as a function of UV illumination time for a soot-photocatalyst-KBr pellet placed in the *in situ* reaction cell for following photocatalysts: P25 (red), PC500 (orange), $WO_{3\ Sigma}$ (blue) and $WO_{3\ Mart.}$ (green)

The *in situ* experiment was repeated using visible light LEDs. Under these conditions, the same bands were observed as with UV light for P25 and $WO_{3\ Mart.}$ (positive: CO_2 and $CHOO^-_{(ad)}$; negative: C-H), but for PC500 and $WO_{3\ Sigma}$ no bands could be observed after 10 hours of illumination. The slope of the CO_2 evolution curve (< 10h, @2360 cm^{-1}) was extracted, reflecting the short-term soot mineralization rate of the photocatalysts and is shown in Fig. 10 for both UV and VIS light.

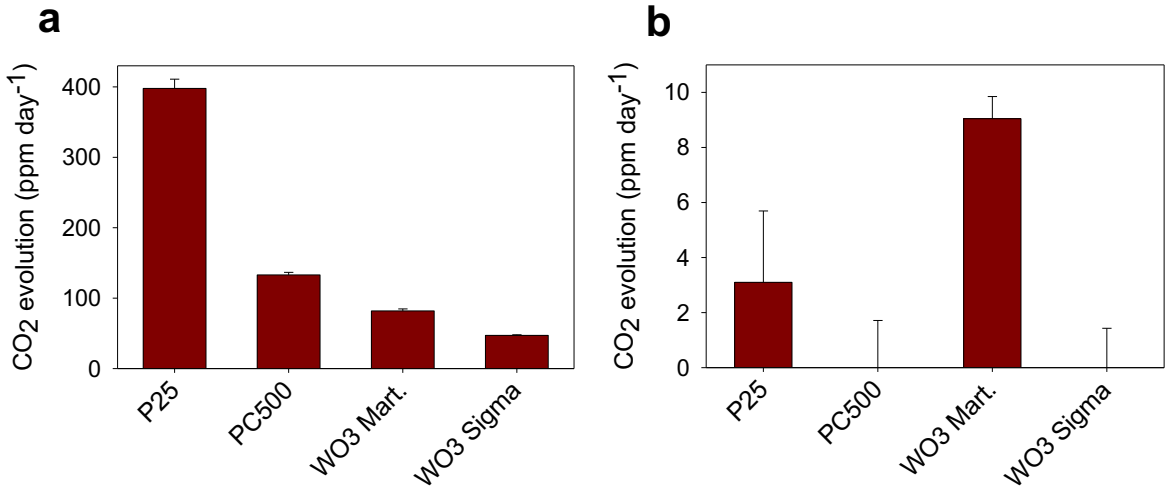

Fig. 10 CO_2 evolution of studied materials based on the *in-situ* soot oxidation detection method when using a) UV and b) VIS light

When looking at Fig. 10a it is clear that the short-term or initial mineralization rate under UV light is the highest for P25. PC500 has the second highest initial mineralization rate, 3 times lower than that of P25, followed by $WO_{3\ Mart.}$, with the lowest initial mineralisation rate obtained with $WO_{3\ Sigma}$. From Fig. 10b a different order can be seen under VIS light, with the highest initial mineralisation rate for $WO_{3\ Mart.}$, followed by P25 and without quantifiable CO_2 formation obtained with PC500 and $WO_{3\ Sigma}$.

It is important to note that it is not possible to directly correlate these results to those obtained in the (long term) digital image analysis experiments above. Both methodologies differ in many ways (*e.g.* substrate, duration, measured parameter). Nevertheless, largely similar trends can still be observed. In the digital image analysis experiments P25 also achieved complete soot oxidation the fastest under UV light, while $WO_{3\ Mart.}$ was also the fastest soot degrader under VIS light.

Besides the initial mineralisation rate, the *in situ* experiments can also be used to assess the specificity of the photocatalytic materials towards full mineralisation of soot into CO_2. This specificity is expressed as the ratio of the absorbance of CO_2 (at 2360 cm^{-1}) to that of formate (at 1360 cm^{-1}) after 10 h of illumination. The result is shown in Table 2 for both UV and VIS light.

Table 2. Absorbance ratio of CO_2 to formate for the four studied photocatalysts when using UV and VIS light

	UV light	VIS light
P25	0.81	0.50
PC500	0.22	N.A.
$WO_{3\ Sigma}$	1.36	N.A.
$WO_{3\ Mart.}$	4.46	2.64

Under both light sources $WO_{3\ Mart.}$ has by far the highest specificity towards CO_2 production, thus resulting in the most complete mineralization after 10 h of UV illumination. In contrast, PC500 has a very low specificity towards full mineralisation, which can be rationalised given its large available surface area but poor electronic properties, that can accommodate a large fraction of less reactive intermediates, without the required photocatalytic power for their fast further degradation.

To summarise, the *in situ* method, just as the image analysis method, showed that under UV light P25 results in the fastest (short term) soot degradation, and under VIS light $WO_{3\ Mart.}$ was the fastest soot degrader, while in terms of specificity $WO_{3\ Mart.}$ performed best under both light sources. When considering real-life applications, the eventual purpose will determine which characteristics are decisive (*e.g.* fast surface cleaning, or prevention of release of toxic compounds).

4. Conclusion

Existing studies on photocatalytic soot degradation focus on TiO_2-based photocatalysts under UV light, which accounts for only ~ 5% of the solar spectrum. In this study the photocatalytic soot oxidation capacity of WO_3-based photocatalysts was studied for the first time under both UV and visible light, along with TiO_2-based benchmark materials. The use of WO_3-based photocatalysts proved to be challenging due to their intrinsic yellow-greenish appearance, that furthermore changed upon progressive illumination. The latter impeded straightforward use of a previously introduced digital image analysis technique for quantifying the degree of soot degradation in a fast and cost-effective manner. As a solution, an additional data processing step is presented, correcting for intrinsic photocatalyst colour changes. This way, the application range of this versatile and accurate detection method has now also been broadened to coloured samples.

Our results have shown that under pure UV light TiO_2-based photocatalysts still outperform WO_3-based materials, both for the degradation of a uniform soot haze as well as for concentrated soot spots, which was further supported by *in situ* experiments. However, under visible light, the lab-synthesized WO_3 photocatalyst was more than two times faster in completely degrading a uniform soot haze, compared to TiO_2, which was also supported by the *in situ* experiments. Similar results were detected for all photocatalysts for the degradation of concentrated soot spots under visible light. When considering the specificity of all materials towards full soot mineralisation into CO_2, again the lab-synthesized WO_3 photocatalysts showed the best performance under both UV and visible light, only generating very small amounts of undesired intermediates. These are first promising results for

utilisation of visible light for energy-efficient photocatalytic soot degradation applying visible light-active photocatalysts such as WO_3.

Declarations

Ethics approval and consent to participate

Not applicable

Consent for publication

Not applicable

Availability of data and materials

The datasets used and/or analysed during the current study are available from the corresponding author on reasonable request.

Competing interests

The authors declare that they have no competing interests

Funding

M.V.H. acknowledges the Research Foundation–Flanders (FWO) for a doctoral fellowship (1135619N).

Authors' contributions

MVH: Conceptualization, Methodology, Data acquisition, Formal analysis, Writing - original draft. **SL:** Supervision, Funding acquisition. **SWV:** Supervision, Funding acquisition, Conceptualization, Writing - review & editing.

References

Braslavsky SE, Braun AM, Cassano AE, et al (2011) Glossary of terms used in photocatalysis and radiation catalysis (IUPAC recommendations 2011). Pure Appl Chem 83:931–1014. https://doi.org/10.1351/PAC-REC-09-09-36

Chabas A, Lombardo T, Cachier H, et al (2008) Behaviour of self-cleaning glass in urban atmosphere. Build Environ 43:2124–2131. https://doi.org/10.1016/j.buildenv.2007.12.008

Chen Q, Li J, Li X, et al (2012) Visible-light responsive photocatalytic fuel cell based on WO3/W photoanode and Cu2O/Cu photocathode for simultaneous wastewater treatment and electricity generation. Environ Sci Technol 46:11451–11458. https://doi.org/10.1021/es302651q

Chin P, Grant CS, Ollis DF (2009) Quantitative photocatalyzed soot oxidation on titanium dioxide. Appl

Catal B Environ 87:220–229. https://doi.org/10.1016/j.apcatb.2008.09.020
Chin P, Roberts GW, Ollis DF (2007) Kinetic Modeling of Photocatalyzed Soot Oxidation on Titanium Dioxide Thin Films. Ind Eng Chem Res 46:7598–7604. https://doi.org/10.1021/ie070083t
Deng X, Yue Y, Gao Z (2002) Gas-phase photo-oxidation of organic compounds over nanosized TiO2 photocatalysts by various preparations. Appl Catal B Environ 39:135–147. https://doi.org/10.1016/S0926-3373(02)00080-2
deRichter R, Caillol S (2011) Fighting global warming: The potential of photocatalysis against CO2, CH4, N2O, CFCs, tropospheric O3, BC and other major contributors to climate change. J Photochem Photobiol C Photochem Rev 12:1–19. https://doi.org/10.1016/j.jphotochemrev.2011.05.002
EEA (2016) Air quality in Europe — 2016 report
Ferrero L, Bigogno A, Cefalì AM, et al (2020) On the synergy between elemental carbon and inorganic ions in the determination of the electrical conductance properties of deposited aerosols: Implications for energy applications. Appl Sci 10:. https://doi.org/10.3390/app10165559
Fukumura T, Sambandan E, Yamashita H (2017) Synthesis and VOC degradation ability of a CeO2/WO3 thin-layer visible-light photocatalyst. Mater Res Bull 94:493–499. https://doi.org/10.1016/j.materresbull.2017.07.003
Hauchecorne B, Terrens D, Verbruggen S, et al (2011) Elucidating the photocatalytic degradation pathway of acetaldehyde: An FTIR in situ study under atmospheric conditions. Appl Catal B Environ 106:630–638. https://doi.org/10.1016/j.apcatb.2011.06.026
Kameya Y, Torii K, Hirai S, Kaviany M (2017) Photocatalytic soot oxidation on TiO 2 microstructured substrate. Chem Eng J 327:831–837. https://doi.org/10.1016/j.cej.2017.06.094
Keulemans M, Verbruggen SW, Hauchecorne B, et al (2016) Activity versus selectivity in photocatalysis: Morphological or electronic properties tipping the scale. J Catal 344:221–228. https://doi.org/10.1016/j.jcat.2016.09.033
Kim J, Choi W (2011) Platinized WO3 as an environmental photocatalyst that generates OH radicals under visible light. Environ Sci Technol 45:3183–3184. https://doi.org/10.1021/es200551x
Lee MC, Choi W (2002) Solid phase photocatalytic reaction on the Soot/TiO2 interface: The role of migrating OH radicals. J Phys Chem B 106:11818–11822. https://doi.org/10.1021/jp026617f
Lee SK, McIntyre S, Mills A (2004) Visible illustration of the direct, lateral and remote photocatalytic destruction of soot by titania. J Photochem Photobiol A Chem 162:203–206. https://doi.org/10.1016/j.nainr.2003.07.002
Luttrell T, Halpegamage S, Tao J, et al (2014) Why is anatase a better photocatalyst TiO 2 films. Sci Rep 4:1–8. https://doi.org/10.1038/srep04043
Martínez DS, Cuéllar EL (2010) Synthesis and characterization of WO3 nanoparticles prepared by the precipitation method: Evaluation of photocatalytic activity under vis-irradiation. Solid State Sci 12:88–94. https://doi.org/10.1016/j.solidstatesciences.2009.10.010
Maury A, De Belie N (2010) State of the art of TiO2 containing cementitious materials: self-cleaning properties. Mater Construcción 60:33–50. https://doi.org/10.3989/mc.2010.48408
Mills A, Wang J, Crow M (2006) Photocatalytic oxidation of soot by P25 TiO2 films. Chemosphere 64:1032–1035. https://doi.org/10.1016/j.chemosphere.2006.01.077
Peeters H, Keulemans M, Nuyts G, et al (2020) Plasmonic gold-embedded TiO2 thin films as photocatalytic self-cleaning coatings. Appl Catal B Environ 267:. https://doi.org/10.1016/j.apcatb.2020.118654
Pozo-Antonio JS, Noya-Pintos D, Sanmartín P (2020) Moving toward smart cities: Evaluation of the self-cleaning properties of si-based consolidants containing nanocrystalline tio2 activated by either uv-a or uv-b radiation. Polymers (Basel) 12:1–20. https://doi.org/10.3390/polym12112577
Rosli NS, Abdullah CAC, Hazan R (2018) Synthesis, characterization and investigation of photocatalytic activity of nano-titania from natural ilmenite with graphite for cigarette smoke degradation. Results Phys 11:72–78. https://doi.org/10.1016/j.rinp.2018.08.032
Sanchez-Martinez D, Martinez-De La Cruz A, Lopez-Cuellar E (2013) Synthesis of WO3 nanoparticles by citric acid-assisted precipitation and evaluation of their photocatalytic properties. Mater Res Bull 48:691–697. https://doi.org/10.1016/j.materresbull.2012.11.024

Smits M, Chan C kit, Tytgat T, et al (2013) Photocatalytic degradation of soot deposition: Self-cleaning effect on titanium dioxide coated cementitious materials. Chem Eng J 222:411–418. https://doi.org/10.1016/j.cej.2013.02.089

Smits M, Huygh D, Craeye B, Lenaerts S (2014) Effect of process parameters on the photocatalytic soot degradation on self-cleaning cementitious materials. Catal Today 230:250–255. https://doi.org/10.1016/j.cattod.2013.10.001

Thorsen WA, Cope WG, Shea D (2004) Bioavailability of PAHs: Effects of Soot Carbon and PAH Source. Environ Sci Technol 38:2029–2037

Van Hal M, De Almeida Campos R, Lenaerts S, et al (2021) Gas phase photofuel cell consisting of WO3- and TiO2-photoanodes and an air-exposed cathode for simultaneous air purification and electricity generation. Appl Catal B Environ 292:120204. https://doi.org/10.1016/j.apcatb.2021.120204

Van Hal M, Verbruggen SW, Yang X, et al (2019) Image analysis and in situ FTIR as complementary detection tools for photocatalytic soot oxidation. Chem Eng J 367:269–277. https://doi.org/10.1016/j.cej.2019.02.154

Verbruggen SW, Keulemans M, Goris B, et al (2016) Plasmonic 'rainbow' photocatalyst with broadband solar light response for environmental applications. Appl Catal B Environ 188:147–153. https://doi.org/10.1016/j.apcatb.2016.02.002

Xie S, Ouyang K (2017) Degradation of refractory organic compounds by photocatalytic fuel cell with solar responsive WO3/FTO photoanode and air-breathing cathode. J Colloid Interface Sci 500:220–227. https://doi.org/10.1016/j.jcis.2017.04.002

Zhang Y, Liao W, Xu P, Hu Z (2012) Visible-Light Responsive Photocatalytic Fuel Cell Based on WO3/W Photoanode and Cu2O/Cu Photocathode for Simultaneous Wastewater Treatment and Electricity Generation. Environ Sci Technol 46:11451–11458. https://doi.org/10.1364/n3.2013.nsa3a.38